Q. J. R. Meteorol. Soc. (2004), **130**, pp. 3207–3222 doi: 10.1256/qj.03.144

Improved mixing representation in Emanuel's convection scheme

By J.-Y. GRANDPEIX[1], V. PHILLIPS[2] and R. TAILLEUX[1,3]*

[1]*Laboratoire Météorologie Dynamique, Jussieu, France*
[2]*Geophysical Fluid Dynamics Laboratory and Princeton University, USA*
[3]*University of Cape Town, South Africa*

(Received 4 August 2003; revised 1 March 2004)

SUMMARY

Recent empirical and modelling studies suggest that mid-tropospheric relative humidity (*RH*) is an important controlling factor of deep atmospheric convection, which appears to be underestimated in present cumulus parametrizations. This indicates the possible presence of shortcomings in the way that entrainment is represented in such parametrizations. This matter was explored in the European Cloud Systems project (EUROCS) by means of an idealized humidity experiment in which the main controlling parameter is *RH*. In the latter study, cloud-resolving model (CRM) experiments suggested that a shallow/deep convection transition occurs when *RH* crosses a threshold value that ranges from about $RH = 50\%$ to $RH = 60\%$.

In this paper, we seek to increase the responsiveness of Emanuel's convection scheme to *RH*, and to reproduce the threshold behaviour of the idealized humidity case, by replacing the original uniform probability density function (PDF) for mixing fractions by a more flexible two-parameter bell-shaped function that allows a wider range of behaviour. The main result is that the parameters of this PDF can be tuned to allow a regime transition to occur near a threshold value of $RH \approx 55\%$. In contrast to CRM results, however, this transition is between two different regimes of deep convection rather than between a shallow and deep regime. Possible ways to obtain a shallow-to-deep transition with Emanuel's scheme are discussed.

KEYWORDS: Cumulus parametrization Entrainment Mixing Tropospheric humidity

1. INTRODUCTION

Recent empirical and modelling studies suggest that mid-tropospheric relative humidity (*RH*) may be an important factor determining the occurrence and intensity of deep atmospheric convection. The physical rationale is that the reduction of buoyancy by entrainment of rising air parcels is bound to be greater for dry environmental air than for more moist air (Raymond 1995; Mapes and Zuidema 1996; Brown and Zhang 1997). For instance, Tompkins (2000) found that convection would tend to recur in regions having previously experienced convection in a comparison of two-dimensional (2D) and three-dimensional (3D) cloud-resolving model (CRM) simulations. It was suggested that this was because such regions were humidified by the convection. Furthermore, he invoked a positive feedback between the moistening of the local environment by convection and the promotion of convection by entrainment of moist environmental air, in order to account for the pronounced large-scale organization in 2D. (Note, however, the alternative view that it is the large-scale lifting—which usually tends to accompany the humidification of the large-scale environment—rather than the humidification itself, that could be the direct cause of the transition to deep convection. Resolving this question is beyond the scope of this paper, however.) To investigate the mechanisms and reality of this hypothesized sensitivity of deep convection to *RH*, Derbyshire *et al.* (2004) (referred to as D04 hereafter) compared the performances of two CRMs and various single-column models (SCMs) on an idealized humidity case in which *RH* is the main controlling parameter of deep convection. This intercomparison revealed a strong sensitivity to *RH* of the two CRMs, which both exhibited a marked shallow/deep

* Corresponding author: LMD-UPMC Paris 6, Case courrier 99, 4 Place Jussieu, 75252 Paris Cédex 05, France.
e-mail: jean-yves.grandpeix@lmd.jussieu.fr

convection transition for a threshold value of *RH* of about 50–60%. The SCMs, on the other hand, were found to be much less responsive, in general, to the value of *RH**.

This lack of responsiveness of the SCMs points naturally to potential shortcomings in the ways the entrainment/detrainment processes and the mass-flux closure are treated in present cumulus parametrizations. In this paper, we only report our efforts regarding the first of these possibilities. The issue of mass flux was considered to be of secondary importance in view of one CRM showing little variation of the mass fluxes at cloud base from one experiment to the other in the simulations reported by D04. On the other hand, the maximum updraught mass fluxes and precipitation rates were found to vary sensitively in the same experiments, which would seem to implicate the mixing processes in the deep-convective response. In this study, which is part of a CRM/SCM intercomparison on an idealized humidity case, we are interested in understanding how to increase the responsiveness to *RH* of Emanuel's (1991, 1993) scheme, which is used in the LMD† climate model. The present study applies equally well to the more recent version of the scheme by Emanuel and Zivkŏvic-Rothman (1999), in which entrainment/detrainment processes are modelled in a similar way.

In Emanuel's convection parametrization, the entrainment process in a given convective cell is intended to be explicitly represented by the spectrum of mixed draughts created by each entrainment event. The procedure is designed to reflect the improved understanding of storm dynamics achieved by the detailed analysis of aircraft observations by Blyth *et al.* (1988). According to their view, deep cumuli possess a multi-thermal structure, and entrainment occurs by environmental air mixing with updraught air that is shed from thermals during their ascent. Their schematic picture appears to be consistent with the idea that lateral entrainment is the primary entrainment mechanism in deep cumuli.

Central to Emanuel's parametrization, as well as to the stochastic mixing model of Raymond and Blyth (1986) upon which it is based, is the probability density function (PDF) for mixing due to entrainment. There is no consensus yet, however, about what this PDF ought to be, owing to the lack of unambiguous experimental data, and *ad hoc* assumptions are often made. Emanuel's scheme assumed a uniform PDF, whereas Raymond and Blyth (1986) assumed a uniform rate of decrease of the probability mixing distribution function with increasing fraction F of environmental air in the mixture. In other parametrizations, such as Kain and Fritsch (1990), the air shed from the undiluted updraught core is assumed to mix with environmental air in almost equal proportions. Specifically, Kain and Fritsch used a centred Gaussian distribution for the probability of mixing, with a mean of 50% and a standard deviation of 20%. For instance, Cohen (2000) inferred a 'U-shaped' anti-Gaussian distribution of mixtures from a numerical simulation of cumulonimbus clouds, having a minimum near $F = 0.5$ and rapidly increasing near $F = 0$ and 1. In this paper, we argue that the choice of the particular form of the PDF is crucial for enhancing the responsiveness of Emanuel's scheme to *RH*. Specifically, our purpose is to show that the *RH* threshold behaviour for the shallow/deep convection transition, in the context of the idealized humidity case of D04, can partly be reproduced by choosing a somewhat more complex mixing PDF than the uniform one assumed by Emanuel. At this stage, we offer only a heuristic justification for this new PDF in sections 2 and 3, since the main purpose is to show that increased responsiveness to *RH* can be achieved in the original framework of Emanuel's parametrization only by

* Note that this characterization in terms of an *RH* threshold is limited, in the idealized humidity case, to target *RH* vertical profiles that are independent of height; dealing with the detailed structure of tropospheric humidity is beyond the scope of this intercomparison case.

† Laboratoire Météorologie Dynamique.

altering the form of the PDF. Further justification, by using CRM data for instance, is left for future work.

As shown further in the text, the CRM results are only partly reproduced in the sense that the new PDF makes it only possible to reproduce the threshold behaviour, but it is between two deep convection regimes, not between a shallow and a deep convection regime. Indeed, this problem arises because, in Emanuel's scheme, the cloud-top height is determined solely by the adiabatic ascent of the undiluted updraught, so that the scheme predicts deep convection independently of how the entrainment/detrainment processes are represented. Redelsperger *et al.* (2002) argued that this is invalid in many cases. This difficulty of Emanuel's scheme can only be overcome by altering the mass-flux closure. Although this is beyond the scope of this paper, we outline the way we think this should be done in the conclusion, based on preliminary results of work currently underway.

The paper is organized as follows. Section 2 outlines the main features of Emanuel's scheme as regards mixing and its relation to the form of the probability mixing distribution. The alternative mixing representation studied in this paper is also presented. Section 3 further details the features of the new PDF. The improvements brought about by the new PDF, and some discussion about its impact on a global scales, are discussed in the final section 4.

2. Entrainment/detrainment in Emanuel's scheme

There are three published versions of Emanuel's scheme (Emanuel 1991, 1993; Emanuel and Zivkŏvic-Rothman 1999). The software code used in the present paper is derived from a code produced by K. Emanuel in 1995, which implements a model very similar to Emanuel's (1993) model. Our version differs from Emanuel's in the removal of most explicit grid dependencies and in the use of ice thermodynamics. Most of these changes are irrelevant for the present study, except the use of ice thermodynamics which strengthens the precipitating downdraughts. Notice, however, that the scheme implemented in the LMDZ Global Climate Model (GCM) (Doutriaux-Boucher and Quaas 2004) used in section 4 does not include ice thermodynamics.

The general structure and the mixing scheme are roughly the same in all versions subsequent to Emanuel (1993) (including Emanuel and Zivkŏvic-Rothman (1999)). However, the description of the mixing scheme is complete only in the 1991 paper. For the sake of clarity, we shall adhere to this description, which is in terms of liquid-water potential temperature, θ_l, although our code corresponds to the 1993 description, which is in terms of liquid-water static energy h.

(*a*) *Structure and basic principles*

The backbone of Emanuel's scheme is a region of adiabatic ascent originating from a low-level layer and ending at its level of neutral buoyancy. Shedding from this adiabatic ascent yields, at each level, a set of draughts which are mixtures of adiabatic ascent air—from which some precipitation is removed—with environmental air. These mixed draughts move adiabatically up or down to levels where, after further removal of precipitation and evaporation of cloudy water, they are at rest at their new levels of neutral buoyancy.

To be more explicit, we follow Emanuel (1991) and express the thermodynamic properties of mixtures in terms of liquid-water potential temperature. Let θ_{la} be the liquid-water potential temperature of the region of adiabatic ascent and $T_a(z)$ its temperature. Then air shed by the adiabatic ascent at level z_0 will have a liquid-water potential

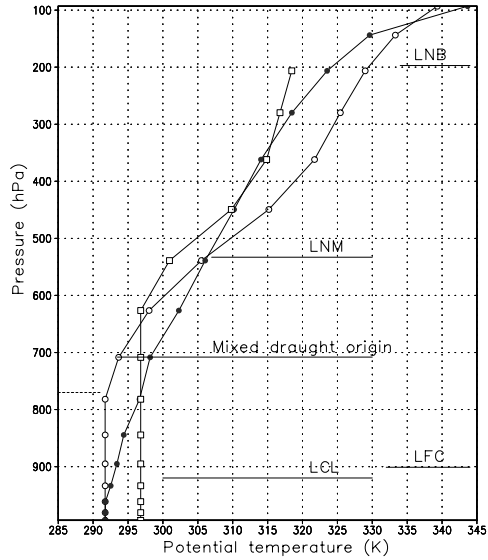

Figure 1. Example of liquid-water potential-temperature profiles for the environment, $\widetilde{\theta}(z)$, (dark circles), the air shed from adiabatic ascent after removal of precipitation, $\theta'_{\rm la}(z)$, (open circles), and the mixed draught originating from the 700 hPa level with mixing fraction 0.7, $\theta'_{\rm lm}(z_0, 0.7, z)$, (open squares). The first two curves intersect at the level of neutral mixing (LNM), and the mixed-draught and environment curves intersect at three levels of neutral buoyancy, the lower and upper ones being detrainment levels.

temperature that is expressed as:

$$\theta'_{\rm la}(z_0) = \theta_{\rm la} \exp\left\{\frac{L_{\rm v} l_{\rm pa}(z_0)}{C_{\rm pd} T_{\rm a}(z_0)}\right\},$$

where $L_{\rm v}$ is the latent heat of vaporization, $C_{\rm pd}$ is the heat capacity per unit mass of dry air and $l_{\rm pa}(z_0)$ is the amount of water precipitated at z_0 (see Fig. (1) for an example of a $\theta'_{\rm la}(z)$-profile). Here, $l_{\rm pa}(z)$ is expressed in terms of a conversion rate to precipitation, $\epsilon_{\rm p}(z)$, and the amount, $q_{\rm la}(z)$, of liquid water in the adiabatic updraught:

$$l_{\rm pa}(z) = \epsilon_{\rm p}(z) q_{\rm la}(z).$$

The conversion rate, $\epsilon_{\rm p}(z)$, varies among different versions of Emanuel's scheme. In the present paper, the 1991 formulation is adhered to, with $\epsilon_{\rm p}$ varying linearly from 0 to $\epsilon_{\rm max}$ between $p^{\rm c} = 150$ hPa and $p^{\rm t} = 500$ hPa above the lifting condensation level (LCL), and is constant elsewhere. There is a slight difference between our scheme and Emanuel's one: Emanuel uses $\epsilon_{\rm max} = 1$ while we use $\epsilon_{\rm max} = 0.995$, which yields a better simulation of moistening at cloud top.

The liquid-water potential temperature, $\theta_{\rm lm}(z_0, F)$, of mixed draughts originating at z_0 with mixing fraction F is a weighted average of the environment potential temperature, $\widetilde{\theta}(z_0)$, and of $\theta'_{\rm la}(z_0)$:

$$\theta_{\rm lm}(z_0, F) = F\widetilde{\theta}(z_0) + (1 - F)\theta'_{\rm la}(z_0),$$

(Eq. (2) of Emanuel (1991)—but notice the change in notation: Emanuel denotes σ^{ij} the mixing fraction of draughts originating at level i and detraining at level j; we use the generic name F for all mixing fractions). On the (θ, z) plot of Fig. 1, points representing mixtures generated at z_0 cover the segment joining $\widetilde{\theta}$ and $\theta'_{\rm la}$ profiles. Levels where the

two profiles intersect are singular points where all mixtures have the same liquid-water potential temperature. These levels of neutral mixing (LNMs) are to play a key role when analysing detrainment levels of mixed draughts.

Mixed draughts generated at level z_0 will detrain at levels, z_1. These levels are such that the environmental potential temperature, $\widetilde{\theta}(z_1)$, is equal to the liquid-water potential temperature of the mixed draught after precipitation has been removed (see paragraph (d) below in this section):

$$\begin{aligned} \widetilde{\theta}(z_1) &= \theta'_{\mathrm{lm}}(z_0,\, F,\, z_1) \\ \theta'_{\mathrm{lm}}(z_0,\, F,\, z_1) &= \theta_{\mathrm{lm}}(z_0,\, F)\, \exp\left\{\frac{L_{\mathrm{v}} l_{\mathrm{pm}}(z_0,\, F,\, z_1)}{C_{\mathrm{pd}} T_{\mathrm{m}}(z_1)}\right\}. \end{aligned} \tag{1}$$

(We use the same notations for the mixed draughts that we used for the adiabatic updraught, merely replacing the subscript 'a' by 'm'.)

Here, $l_{\mathrm{pm}}(z_0,\, F,\, z_1)$ is the amount of water precipitated at z_1 (see Fig. 1 for a draught characterized by $\theta'_{\mathrm{lm}}(z_0,\, F,\, z)$). Following Emanuel (1993), $l_{\mathrm{pm}}(z_0,\, F,\, z_1)$ is parametrized as the excess of liquid water in the mixed draught relative to the liquid water in the adiabatic updraught after precipitation has been removed: $l_{\mathrm{pm}}(z_0,\, F,\, z_1) = q_{\mathrm{lm}}(z_0,\, F,\, z_1) - \{1 - \epsilon_{\mathrm{p}}(z_1)\} q_{\mathrm{la}}(z_1)$. The determination of z_1 from Eq. (1) has been described by Emanuel (1991).

Obviously, the behaviour of mixing processes depends strongly on the parametrization of precipitation. Nevertheless, formal developments and qualitative analysis of simulation results should be valid for a wide range of parametrizations.

(*b*) *Statistical representation of mixing*

Let m_{a} be the mass shed by the adiabatic ascent within a given layer $[z,\, z + \delta z]$ during a given time interval δt. This mass is mixed with environmental air to build a set of mixtures.

(i) *Discrete description of mixture samples.* Consider a given (finite) sample of mixed fluid made of a mass δm_{a} of adiabatic ascent air and a mass δm_{e} of entrained environmental air. It has a total mass $\delta m_{\mathrm{t}} = \delta m_{\mathrm{a}} + \delta m_{\mathrm{e}}$. The mixing fraction of environmental air in the sample is $F = \delta m_{\mathrm{e}} / \delta m_{\mathrm{t}}$. All these variables may be expressed in terms of δm_{a} and F:

$$\begin{aligned} \delta m_{\mathrm{e}} &= \frac{F}{1 - F} \delta m_{\mathrm{a}}, \\ \delta m_{\mathrm{t}} &= \frac{1}{1 - F} \delta m_{\mathrm{a}}. \end{aligned} \tag{2}$$

For infinitesimal samples these formulae become:

$$\begin{aligned} \mathrm{d}m_{\mathrm{e}} &= \frac{F}{1 - F} \mathrm{d}m_{\mathrm{a}}, \\ \mathrm{d}m_{\mathrm{t}} &= \frac{1}{1 - F} \mathrm{d}m_{\mathrm{a}}. \end{aligned} \tag{3}$$

(ii) *Continuous description of mixtures.* When dealing with continuous variables, a distribution variable has first to be chosen. Following Emanuel (1991), we use the mixing fraction F as distribution variable in order to describe the set of mixtures. More precisely, their statistical properties will be described by the spectral densities with respect to F of the various masses: $\mathrm{d}m_{\mathrm{a}}/\mathrm{d}F$, $\mathrm{d}m_{\mathrm{e}}/\mathrm{d}F$, $\mathrm{d}m_{\mathrm{t}}/\mathrm{d}F$.

These spectral densities are usually parametrized in terms of the PDF, $P(F)$, describing the distribution of air shed from the region of adiabatic ascent over the range of F, the integral of $P(F)$ being unity (see Emanuel (1991) or Zhao and Austin (2003) for a review). In terms of $P(F)$, the various spectral densities read:

$$\begin{aligned} \frac{\mathrm{d}m_\mathrm{a}}{\mathrm{d}F} &= m_\mathrm{a} P(F), \\ \frac{\mathrm{d}m_\mathrm{e}}{\mathrm{d}F} &= m_\mathrm{a} \frac{F P(F)}{1-F}, \\ \frac{\mathrm{d}m_\mathrm{t}}{\mathrm{d}F} &= m_\mathrm{a} \frac{P(F)}{1-F}, \end{aligned} \tag{4}$$

where we have used Eqs. (3). From the last of these relations, it is obvious that the total mass of the mixtures will be finite if and only if $P(F)$ is such that the integral $\int_0^1 P(F)/(1-F)\,\mathrm{d}F$ is convergent. Because of the inconvenience of such a constraint, we use another parametrization.

Let us introduce a function $Q(F)$ such that:

$$\begin{aligned} &P(F) = \dot{Q}(F)(1-F) \quad \text{(where the dot denotes the derivative)}, \\ &Q(0) = 0. \end{aligned} \tag{5}$$

It is easy to prove that Q is non-decreasing and that its integral is unity. Conversely, for any non-decreasing function, Q, defined over the interval [0, 1] such that its integral is unity and $Q(0) = 0$, $P(F)$ defined by Eqs. (5) is a PDF and yields finite masses of mixtures. The various spectral densities expressed in terms of $Q(F)$ are:

$$\begin{aligned} \frac{\mathrm{d}m_\mathrm{a}}{\mathrm{d}F} &= m_\mathrm{a}(1-F)\dot{Q}(F), \\ \frac{\mathrm{d}m_\mathrm{e}}{\mathrm{d}F} &= m_\mathrm{a} F \dot{Q}(F), \\ \frac{\mathrm{d}m_\mathrm{t}}{\mathrm{d}F} &= m_\mathrm{a} \dot{Q}(F). \end{aligned} \tag{6}$$

Integration of the last of these equations yields the total mass of the mixtures, $m_\mathrm{t} = m_\mathrm{a} Q(1)$, which shows that the entrainment rate is proportional to $Q(1)$. It is also evident that an interpretation of $Q(F)$ may be derived from these formulae: $\dot{Q}(F)/Q(1)$ is the PDF describing the distribution of the mixture mass m_t over the range of F.

(*c*) *Examples of PDFs*

Emanuel uses a uniform $P(F)$ on $[0, 1-\epsilon]$, with $\epsilon = 0.05$. This corresponds to:

$$\begin{aligned} Q(F) &= -\frac{\ln(1-F)}{1-\epsilon} \quad \text{if } F < 1-\epsilon, \\ &= -\frac{\ln(\epsilon)}{1-\epsilon} \qquad \text{if } F > 1-\epsilon. \end{aligned} \tag{7}$$

$Q(1)$ is of the order of 3.

The present study uses for $Q(F)$ a family of S-shaped functions (i.e. smoothed step functions), with two parameters: F_0 is the centre of the step and Γ is the width of the step

$$Q(F) = \frac{1}{a}\left\{\tanh\left(\frac{F-F_0}{\Gamma}\right) + \tanh\left(\frac{F_0}{\Gamma}\right)\right\}. \tag{8}$$

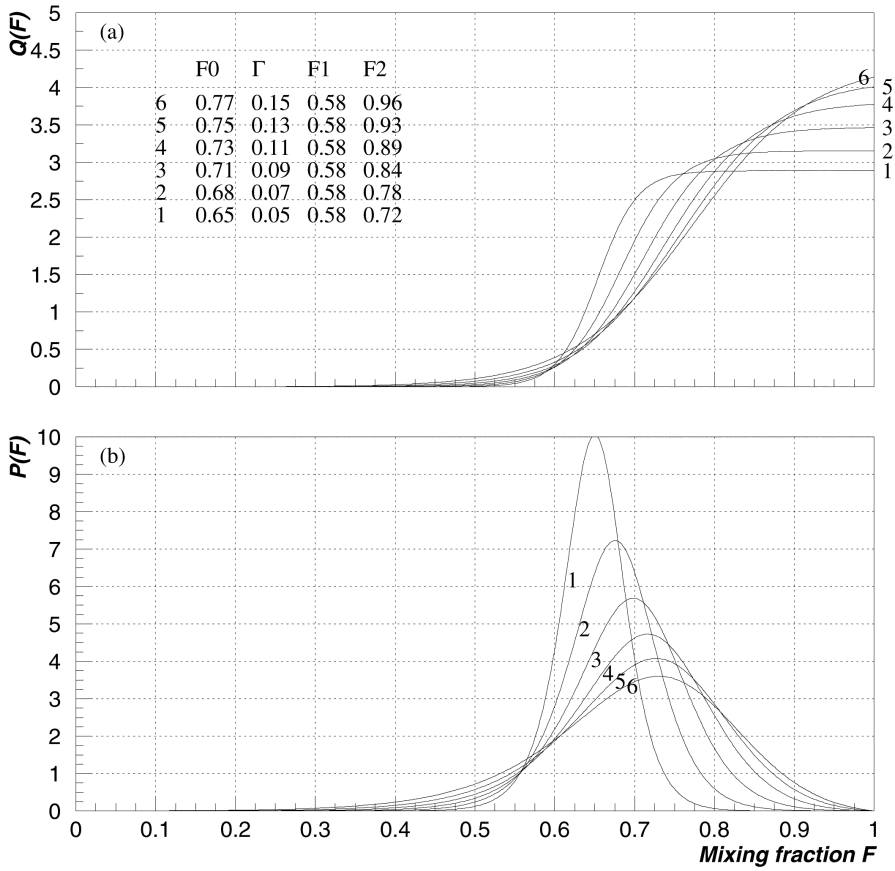

Figure 2. Functions (a) $Q(F)$ and (b) $P(F)$ for various values of F_0 and Γ; $[F_1, F_2]$ is the interval centred at F_0 in which 90% of Q variation occurs.

Here, a is a normalization factor such that the integral of $Q(F)$ is unity:

$$a = \tanh\left(\frac{F_0}{\Gamma}\right) + \Gamma \ln\left[\frac{\cosh\{(1-F_0)/\Gamma\}}{\cosh(F_0/\Gamma)}\right].$$

Instead of F_0 and Γ, one may characterize these laws by the F-interval in which lies 90% of the mixture mass: namely, the interval $[F_1, F_2]$, whose middle is F_0, such that $Q(F_2) - Q(F_1) = 0.9Q(1)$. Approximately, if F_2 is below 0.9, the relation between (F_0, Γ) and (F_1, F_2) is expressed as:

$$\begin{aligned} F_0 &= (F_1 + F_2)/2, \\ F_1 - F_2 &\simeq 3\Gamma. \end{aligned} \tag{9}$$

Figure 2 displays some instances of $Q(F)$ and $P(F)$. Curve 1 is the final choice of this study. Curves 2 and 3 have same threshold value, F_1, as curve 1.

One should notice that the two probability distributions, the original Emanuel (1991) one and our final choice ($F_0 = 0.65$, $\Gamma = 0.05$), yield $Q(1) \simeq 3$, i.e. they yield similar entrainment rates, differing mainly by their widths, the new distribution being much narrower (width $\simeq 0.15$) than the original one (width $\simeq 0.9$).

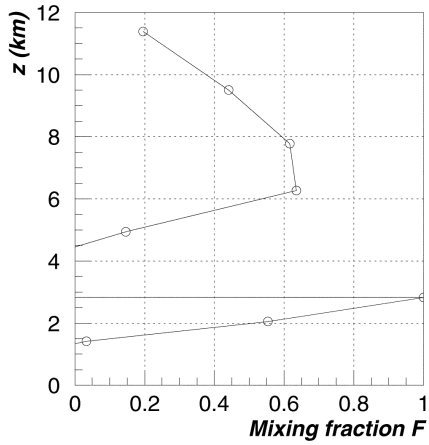

Figure 3. Example of the neutral-buoyancy level (after precipitation removal and cloud-water evaporation) as a function of mixing fraction, F, for mixtures originating from the 3 km level.

(*d*) *Mixed-draught destination*

(i) *Mixed draughts originating below the level of neutral mixing (LNM).* Consider mixtures originating at a level (z_i) below the LNM. Liquid-water potential temperatures of all mixtures lie between $\widetilde{\theta}_{\text{surf}}$ and $\widetilde{\theta}(i)$. Hence, all of the mixtures have a level of neutral buoyancy below z_i. However, most of them have also (at least) one level of neutral buoyancy above z_i (see Fig. 3 for an instance of a curve of the neutral buoyancy level as a function of F). The double-valued upper branch can be qualitatively explained: (1) levels of neutral buoyancy close to z_i correspond to mixtures containing enough liquid water to start precipitating as soon as they leave z_i, i.e. to mixtures with a high proportion of adiabatic ascent air; (2) mixtures with higher value of F need some lifting (so that enough water is precipitated) before reaching their level of neutral buoyancy; (3) very high levels of neutral buoyancy correspond to mixtures containing a high amount of water, that is, mixtures with very low values of F.

In summary, for most of the domain of F, mixtures have three levels of neutral buoyancy, one below and two above (except, possibly, for an interval close to $F = 1$ whose corresponding mixtures may only descend).

In order to deal with this multiplicity, Emanuel's scheme determines a critical mixing fraction, F_{crit}, equal to the negative buoyancy limit of the mixtures, and applies the following rule: (1) mixtures with $F > F_{\text{crit}}$ yield downdraughts; (2) mixtures with $F < F_{\text{crit}}$ yield updraughts ending at their highest level of neutral buoyancy. This rule is used also in the present model.

(ii) *Mixed draughts originating above the LNM.* The liquid-water potential temperature of mixtures generated at a level, z_j, above the LNM is always higher than $\widetilde{\theta}(j)$. Hence, all of them have their level of neutral buoyancy above z_j (and it turns out that there is only one). Thus, mixing processes above the LNM may yield only updraughts.

(iii) *Neutral mixtures.* Due to vertical discretization, some mixtures detrain within the very grid level from which they originate. These neutral mixtures are handled differently in the present scheme and in the original Emanuel's scheme: (1) in Emanuel's scheme they are ignored and the rest of the mixed mass fluxes are renormalized so as to ensure mass conservation; (2) in the present scheme these neutral mixtures are taken

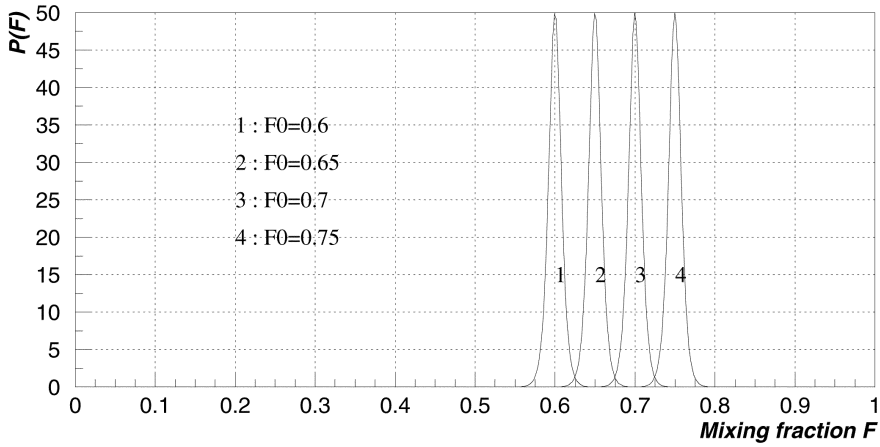

Figure 4. Samples of narrow probability density functions ($\Gamma = 0.01$) used for F-space scanning.

into account. At some level, more than half of the mass shed by the adiabatic ascent may go into them. However, accounting for them does not appear to be a key factor (see section 3).

(iv) *Consequences for the expected sensitivity of mixed-draught mass fluxes to* F_1. Since all mixed draughts originating above the LNM are ascending, one does not expect dramatic effects for these draughts when $Q(F)$ is changed. The situation is quite different for draughts originating below the LNM; varying the $[F_1,\ F_2]$ interval from low to high values of F may cause a situation where there are only updraughts to be replaced by a situation where there are only downdraughts. Moreover, the lower bound of the F-interval yielding downdraughts is an increasing function of mid-tropospheric relative humidity. Thus one may expect that, for a PDF concentrated at high values of F, there will exist a threshold of mid-tropospheric relative humidity below which all mixtures generated below the LNM will yield downdraughts. Designing such a probability law and tuning it to fit CRM results is the purpose of the next section of this paper.

3. PDF DETERMINATION

The objective here is to determine F_1 by requiring that the *RH* threshold mentioned in the previous section be comparable with that for the transition between shallow and deep convection simulated by CRMs, i.e. $RH \simeq 50\%$ to 60%. Then F_2 is to be determined from properties of high-F mixtures and from the study of vertical mass-flux profiles.

In order to perform these studies, separate contributions due to various values of F must be analysed. Thus, a set of simulations are performed using narrow PDFs ($\Gamma = 0.01$) centred at incremental F_0 values (see Fig. 4). Since the environmental temperature and humidity are nudged towards fixed target profiles, they do not vary much between the various simulations (in fact, it was verified that they were nearly constant). Now, saturated mass fluxes, precipitation sources and heating due to saturated draughts all combine linearly when PDFs are combined linearly. This is due to the structure of Emanuel's scheme; the saturated mass fluxes are just the sum of mass-flux contributions due to each F-value, and the tendencies due to the cloud part are the sums of tendency contributions due to each saturated mass flux. This is not true for

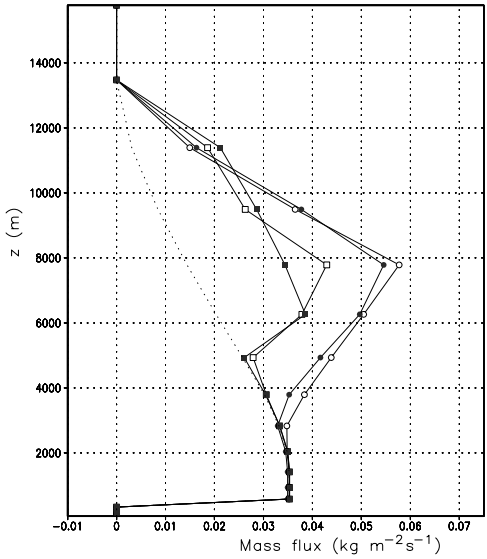

Figure 5. Updraught mass-flux profiles for $RH = 70\%$ and $\Gamma = 0.01$, for $F_0 = 0.55$ (open circles), $F_0 = 0.6$ (dark circles), $F_0 = 0.65$ (open squares), and $F_0 = 0.7$ (dark squares), together with the adiabatic updraught mass flux (dotted line).

unsaturated draughts; they do not depend linearly on saturated mass fluxes. However, since subcloud-layer conditions are found to vary only weakly between simulations and since mid-tropospheric effects are cancelled out by nudging, a nearly linear behaviour for unsaturated downdraughts may be assumed.

(*a*) *Scanning F_0 space by 0.05 steps, using a narrow PDF ($\Gamma = 0.01$)*

Figure 5 displays vertical profiles of total updraught mass fluxes that are obtained once a steady state has been reached in four simulations of the $RH = 0.7$ case, for four values of F_0 (0.55, 0.60, 0.65, 0.70). The LNM is located slightly below 5500 m. The leftmost curve (dotted) is the mass flux of adiabatic ascent. The first striking result of this plot is that the mixed updraught mass fluxes, which are the differences between the total mass fluxes and the adiabatic-ascent mass flux, are negligible below the LNM for $F_0 > 0.70$ but are important for $F_0 < 0.65$. This threshold behaviour is found to occur at all values of RH. For instance, Fig. 6 displays updraught mass-flux profiles for the $RH = 90\%$ case. The threshold above which sub-LNM mixed updraughts are absent is then between $F_0 = 0.75$ and $F_0 = 0.8$. By performing this procedure for various RH cases, it is possible to define the function $F_{\text{threshold}}(RH)$ displayed in Fig. 7.

The second striking feature in the plots of updraught mass flux is the weird shape of the profiles when $F_0 > F_{\text{threshold}}$. This 'mushroom' shape is due to the fact that mixed draughts originating above the LNM are always ascending, irrespective of their mixing fraction F and relative humidity. In this parametrization, where the height of the convective column is independent of the entrainment process, such behaviour is unavoidable.

(i) *F_1 determination.* Since CRM simulations suggest that convection is much weaker for $RH < 0.5$ than for $RH > 0.6$, one may infer from Fig. 7 that F_1 is of the order of 0.6.

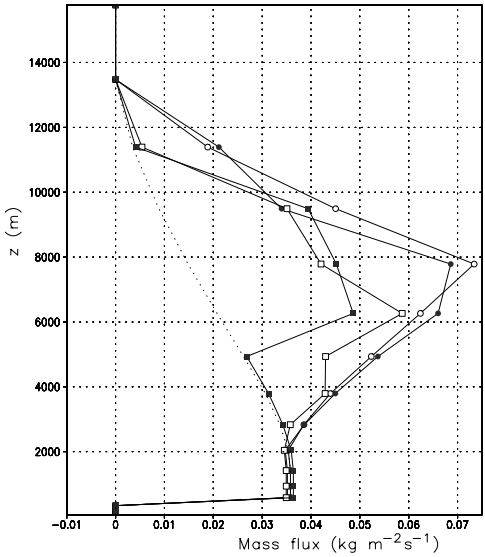

Figure 6. Updraught mass-flux profiles for $RH = 90\%$ and $\Gamma = 0.01$, for $F_0 = 0.65$ (open circles), $F_0 = 0.70$ (dark circles), $F_0 = 0.75$ (open squares), and $F_0 = 0.80$ (dark squares), together with the adiabatic updraught mass flux (dotted line).

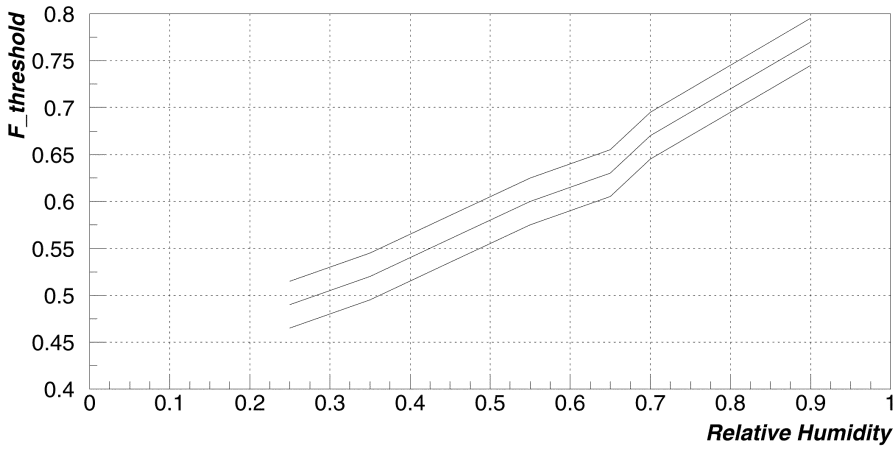

Figure 7. Estimated threshold F-value as a function of relative humidity, together with the upper and lower bounds of the estimate.

(ii) *F_2 determination* Both mass-flux profiles in Figs. 5 and 6 show that the altitude of maximum mass flux decreases as F_0 increases (although this is a rather crude visualization of the behaviour of the altitude of the maximum since only two levels are involved); it varies from 7500 m for $F_0 \simeq 0.65$ to 6500 m for $F_0 \simeq 0.75$. From the altitude of the maximum of upward mass flux predicted in the CRM simulations, which is close to 6000 m (see D04, Fig. 4), one may infer that high-F mixtures must yield an important fraction of mixed draughts, so that F_2 ought to be as high as possible.

On the other hand, scanning F_2 space for fixed F_1 shows that mass-flux sensitivity to RH decreases when F_2 increases; the rate of change of the maximum updraught mass flux, $\Delta M_{\mathrm{up,max}}/\Delta RH$, changes from 0.05 kg m^{-2}s^{-1} down to 0.03 kg m^{-2}s^{-1} when F_2

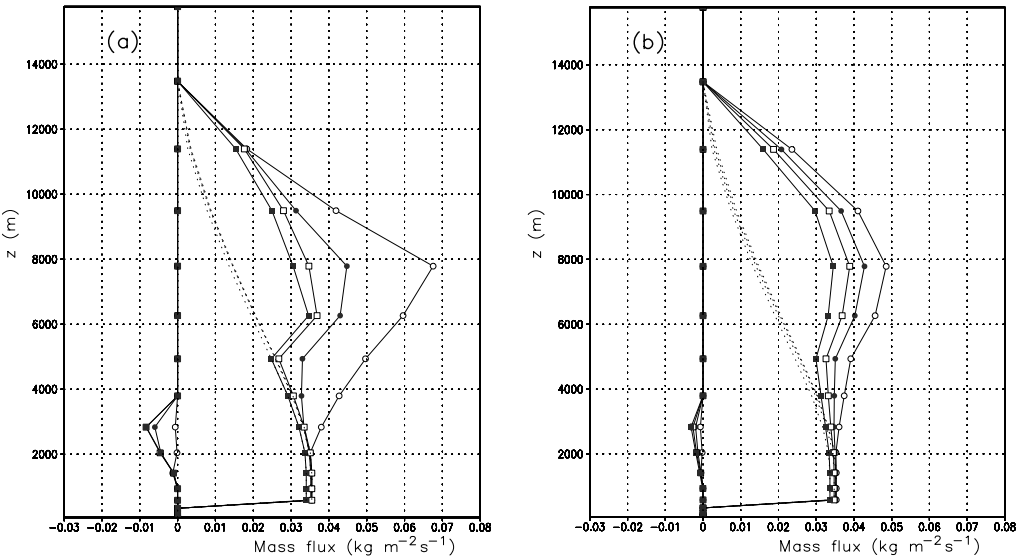

Figure 8. Vertical saturated updraught (rightmost lines) and downdraught (leftmost lines) mass-flux profiles obtained with (a) the final PDF ($F_0 = 0.65$, $\Gamma = 0.05$) and (b) the uniform PDF, for $RH = 0.9$ (open circles), $RH = 0.7$ (dark circles), $RH = 0.5$ (open squares) and $RH = 0.25$ (dark squares), together with the adiabatic mass fluxes (dotted lines).

varies from 0.72 to 0.93. This is in qualitative agreement with the shapes of the $P(F)$ curves in Fig. 2—the higher F_2, the smoother the threshold.

From these results, one may roughly estimate that the possible interval for F_2 values is [0.7, 0.8].

(*b*) *Final PDF*

The final PDF parameters are $F_0 = 0.65$, $\Gamma = 0.05$. The corresponding interval is $F_1 = 0.58$, $F_2 = 0.72$. This yields precipitation rates ranging from 12 mm d^{-1} to 27 mm d^{-1} when mid-tropospheric humidity varies from $RH = 25\%$ to $RH = 90\%$ (to be compared with the range obtained from the standard mixing scheme: from 13 mm d^{-1} to 17 mm d^{-1}). Saturated updraught and downdraught mass-flux profiles are displayed in Fig. 8(a). The total absence of mixed updraughts below the LNM (i.e. below 5500 m) for $RH = 0.25$ and $RH = 0.5$, and the build-up of these updraughts when RH increases above 60%, is the threshold behaviour that was sought for. In contrast, simulations using a uniform PDF (Fig. 8(b)) and simulations using the original mixing scheme (see D04, Fig. 10) yield a weak sensitivity to RH.

Comment on the altitude of the maximum of the updraught mass flux. Since the LNM plays an important role in the mixing model, and since it is dependant upon the parametrization of the microphysics, one might expect the shape of the updraught mass-flux profile to vary with microphysics parameters. We tested this hypothesis within the very restricted framework of Emanuel's (1991) parametrization of the conversion to precipitation. The sensitivity test consisted in varying the critical pressures p^c and p^t by a same amount δp.The main results of this sensitivity test are: (1) the altitude of the maximum of the updraught mass-flux profile depends weakly on δp; (2) saturated downdraught mass fluxes are decreasing functions of δp; for $\delta p \simeq -100$ hPa, downdraughts are very strong and updraughts are unreasonably weak;

for $\delta p \simeq 100$ hPa, downdraughts disappear and there is no longer any sensitivity to *RH*. To sum up, the acceptable domain for δp goes from -50 hPa (yielding an altitude of the mass-flux maximum that is too high) to 50 hPa (yielding a slightly lower altitude of the maximum and a weaker sensitivity). The present microphysics parametrization is too crude for a finer analysis. However, this very simple test shows that it may be meaningful to consider lowering the LNM while using some more elaborate microphysics (the one used by Emanuel and Zivkŏvic-Rothman (1999) could be a first step).

4. Results and discussion

As shown by D04, current cumulus parametrizations seem to underestimate the sensitivity of atmospheric deep convection to the details of the vertical profile of mid-troposphere *RH*, pointing to potential shortcomings in the way entrainment is represented in such parametrizations. The idealized humidity case, proposed by D04 for investigating this issue, constitutes a very convenient testbed to explore new ways of improving the representation of entrainment in cumulus parametrizations, because the sensitivity to *RH* in this idealized case can be simply characterized by the existence of a threshold behaviour resulting in a shallow/deep convection transition occurring for a *RH* value of about 50–60%. Arguably, the sensitivity of deep convection to realistic *RH* vertical profiles, which may vary significantly with height, probably lacks such a simple characterization. Consequently, it appears justified to seek improvements that are able to reproduce the threshold behaviour within the restricted settings of D04, as a first step towards understanding and improving the sensitivity of cumulus parametrizations to *RH*. Such a strategy was carried out in this paper, in the particular case of Emanuel's scheme, by modifying the PDF that represents how the region of adiabatic undilute ascent is to mix with environmental air. Specifically, we replaced the original uniform PDF used by Emanuel (1991) by a more flexible two-parameter bell-shaped function, and carried out an extensive exploration of the parameter space. Our main conclusions are:

- A high sensitivity of simulated convection to *RH* is obtained by requiring that mixtures generated in deep convection are mostly made of environmental air. This is implemented, thanks to a probability distribution of the mixing fraction of environmental air peaking at values greater than 50%. Our approach thus departs from most buoyancy sorting schemes (see Zhao and Austin (2003) for a survey of PDFs) whose draughts contain, in general, much less environmental air, making the schemes much less sensitive to *RH*.
- The new PDF makes it possible to achieve a regime transition for a threshold value of $RH \approx 0.55$. In contrast to CRM results, however, this regime transition does not describe a shallow/deep transition, but one involving two distinct deep convection regimes acting within the altitude range [3 km, 5 km] (that is, between the level where entrainment becomes important and the level of neutral mixing). For $RH < 0.55$, deep convection is characterized by the undilute updraught being surrounded by multiple saturated downdraughts, whereas for $RH > 0.55$, the undilute updraught is predominantly surrounded by secondary updraughts which contribute significantly to the mass flux and the precipitation rates.
- In order to assess the global impact of the new scheme on the climate simulated by the LMDZ GCM, we performed two four-year simulations with the new and standard versions of the mixing scheme. We found that the mean climatological features, such as the ITCZ and the land/ocean contrast, were little altered by the new scheme (not shown). Differences were found, however, in specific features known to be affected by mid-tropospheric humidity, such as the onset of the West

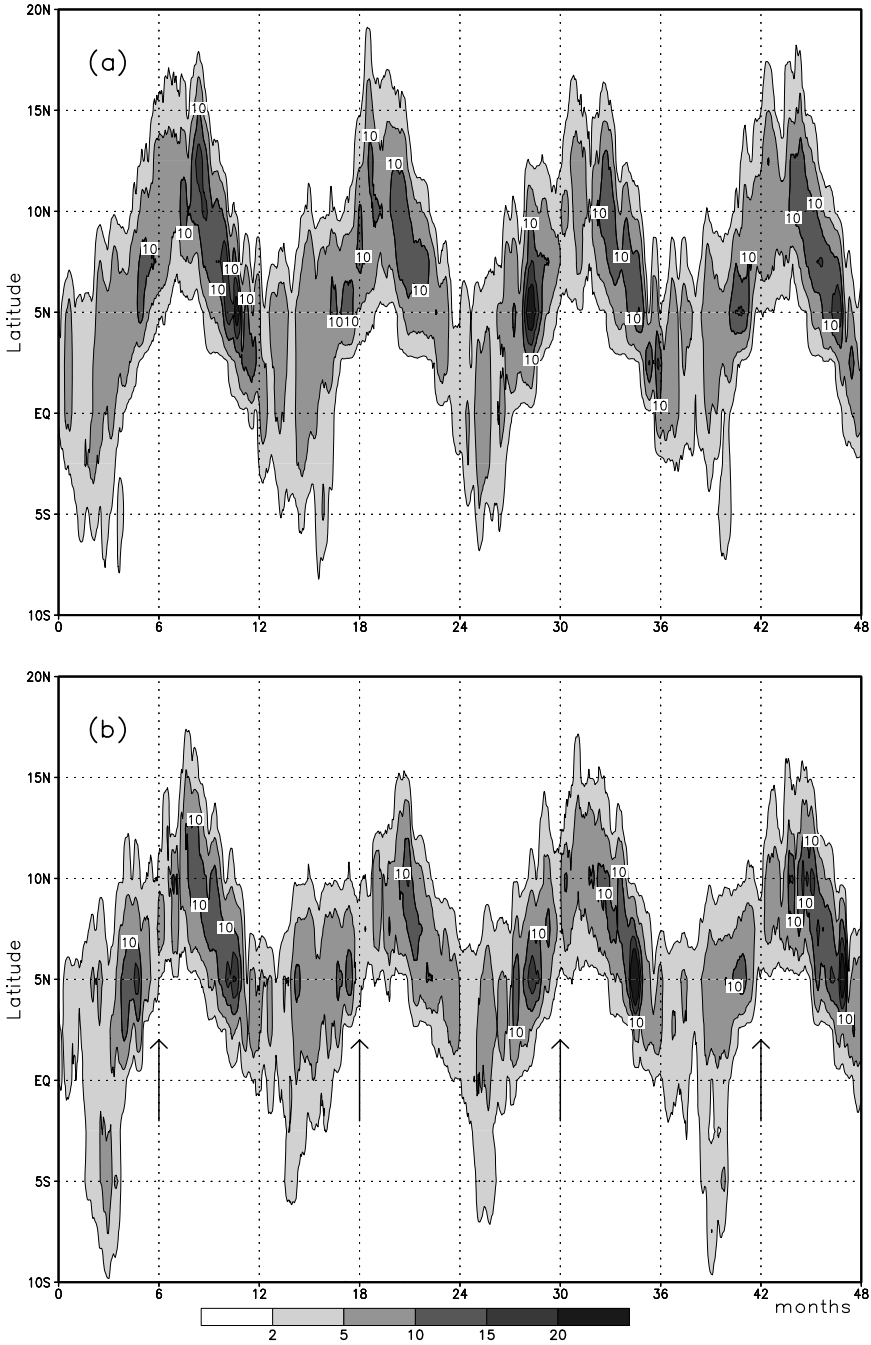

Figure 9. Average precipitation (mm d^{-1}) between 10°W and 10°E from January 1990 to December 1993 (abscissa = months after 1 Jan 1990); (a) the standard LMDZ.3.3 version of Emanuel's convective scheme, and (b) the convective scheme with improved mixing—the monsoon break (a precipitation pause followed by a jump of precipitation maximum from 5°N to 10°N) is clearly visible at the end of June (see vertical arrows in panel (b)), except in 1992.

African monsoon (see, for instance, Sultan and Janicot (2003) for an account of the role of free troposphere dryness on monsoon dynamics). To illustrate this point, we depicted the seasonal cycle of precipitation over West Africa in Fig. 9, for the standard (top) and revised (bottom) versions of the mixing parametrization.

In the simulation using the standard scheme, the simulated latitude of the ITCZ evolves uninterruptedly from 5°N to 10°N during the months of May, June, and July, making it hard to pick up the monsoon onset. In contrast, observations suggest that the ITCZ remains around 5°N until the end of June, when precipitation decreases temporarily before increasing sharply further north, giving the impression of an abrupt shift to around 10°N, marking the onset of the West African monsoon. The new scheme appears to be able to reproduce this observed feature, as emphasized in the bottom panel by the vertical arrows, in three out of the four years simulated.

As said in the introduction, the shallow/deep regime transition obtained in the idealized humidity case cannot be achieved within Emanuel's scheme, because what determines the cloud-top height in this parametrization is entirely determined by the adiabatic ascent of the undiluted updraught. As recently discussed by Redelsperger *et al.* (2002), there are many cases where this approach is invalid, and it seems necessary to modify it. Efforts currently underway consist in fixing the cloud-top height and the vertical variation of the mass flux based on the nature of the mixed draughts. The physical basis for our approach is that the height of the main cloud is likely to be limited by whether the mixed draughts continue to rise as updraughts, or transform into downdraughts heavier than the environment. Specifically, we expect the latter case (found to occur here for $RH < 0.55$) to be associated with a strong reduction in cloud-top height, and hence to shallower convection than in the former case occuring for $RH > 0.55$. Following such a strategy makes it potentially possible to transform the present deep convection regime occuring for $RH < 0.55$ into a shallow convection regime, the situation for $RH > 0.55$ being little altered. Notice, however, that achieving this kind of transition within Emanuel's (1991) scheme may imply changes in the scheme closure. Preliminary research along these lines appears to be satisfactory, and will be reported in a subsequent paper.

ACKNOWLEDGEMENTS

This work was made possible by the European Union grant EVK2 CT1999 0005. The authors acknowledge useful and stimulating interactions with Alain Lahellec. We wish also to thank Sylvain Cheinet and Sebastien Lebonnois, for their help in clarifying statistical matters, and the journal reviewers for very helpful general remarks and close scrutiny. Global simulations were performed at IDRIS (Institut du Developpement et des Ressources en Informatique Scientifique).

REFERENCES

Blyth, A. M., Cooper, W. A. and Jensen, J. B. 1988 A study of the source of entrained air in Montana cumuli. *J. Atmos. Sci.*, **45,** 3944–3964

Brown, R. G. and Zhang, C. 1997 Variability of mid-tropospheric humidity and its effect on cloud-top height distribution during TOGA COARE. *J. Atmos. Sci.*, **54,** 2760–2774

Cohen, C. 2000 A quantitative investigation of entrainment and detrainment in numerically simulated cumulonimbus clouds. *J. Atmos. Sci.*, **57,** 1657–1674

Derbyshire, S. H., Beau, I., Bechtold, P., Grandpeix, J.-Y., Piriou, J.-M., Redelsperger, J.-L. and Soares, P. M. M.	2004	Sensitivity of moist convection to environmental humidity. *Q. J. R. Meteorol. Soc.*, **130,** 3055–3079
Doutriaux-Boucher, M. and Quaas, J.	2004	Evaluation of cloud thermodynamic phase parameterization in the LMDZ GCM by using POLDER satellite data. *Geophys. Res. Lett.*, **31,** 6126–6130
Emanuel, K. A	1991	A scheme for representing cumulus convection in large scale models. *J. Atmos. Sci.*, **48,** 2313–2335
	1993	'A cumulus representation based on the episodic mixing model: the importance of mixing and microphysics in predicting humidity'. Pp. 185–192 in *The representation of cumulus convection in numerical models.* Meteorological Monographs 24, American Meteorological Society, Boston USA
Emanuel, K. A. and Zivkŏvic-Rothman, M.	1999	Development and evaluation of a convection scheme for use in climate models. *J. Atmos. Sci.*, **56,** 1766–1782
Kain, J. S. and Fritsch, J. M.	1990	A one-dimensional entraining/detraining plume model and its application in convective parametrization. *J. Atmos. Sci.*, **47,** 2784–2802
Mapes, B. E. and Zuidema, P.	1996	Radiative–dynamical consequences of dry tongues in the tropical troposphere. *J. Atmos. Sci.*, **53,** 620–638
Raymond, D. J.	1995	Regulation of moist convection over the west Pacific warm pool. *J. Atmos. Sci.*, **52,** 3945–3959
Raymond, D. J. and Blyth, A. M.	1986	A stochastic mixing model for non-precipitating cumulus clouds. *J. Atmos. Sci.*, **43,** 2708–2718
Redelsperger, J.-L., Parsons, D. B. and Guichard, F.	2002	Recovery processes and factors limiting cloud-top height following the arrival of a dry intrusion during TOGA COARE. *J. Atmos. Sci.*, **59,** 2438–2457
Sultan, B. and Janicot, S.	2003	The West African monsoon dynamics. Part II: The 'pre-onset' and the 'onset' of the summer monsoon. *J. Climate*, **16,** 3407–3427
Tompkins, A. M.	2000	The impact of dimensionality on long-term cloud-resolving model simulations. *J. Atmos. Sci.*, **128,** 1521–1535
Zhao, M. and Austin, P. H.	2003	Episodic mixing and buoyancy-sorting representations of shallow convection: A diagnostic study. *J. Atmos. Sci.*, **60,** 892–912